minerals

MDPI

Article

Mg-Phengite in Carbonate Rock Syngenetically Formed from Hydrothermal Fluid: Micro-Textural Evidence and Mineral Chemistry

Chaewon Park [1], Namsoo Kim [1], Sung-Ja Choi [2] and Yungoo Song [1,*]

[1] Department of Earth System Sciences, Yonsei University, Seoul 03722, Korea; parkcw@yonsei.ac.kr (C.P.); nskim@yonsei.ac.kr (N.K.)

[2] Korea Institute of Geoscience and Mineral Resources (KIGAM), Daejeon 34132, Korea; sjchoi@kigam.re.kr

* Correspondence: yungoo@yonsei.ac.kr

Received: 30 June 2020; Accepted: 25 July 2020; Published: 27 July 2020

Abstract: Phengite series is a dioctahedral solid solution between two end-members of muscovite $[K_1[Al_2]^{VI}[Al_1,Si_3]^{IV}O_{10}(OH)_2]$ and celadonite $[K_1[(Fe^{3+},Al)_1,(Mg,Fe^{2+})_1]^{VI}[Si_4]^{IV}O_{10}(OH)_2]$, which have a hetero-valent substitution of $Al^{VI}Al^{IV} \leftrightarrow (Mg, Fe)^{VI}Si^{IV}$. In this study, we report a hydrothermal-originated authigenic Mg-phengite-series mineral, which occurred as polycrystalline aggregates (Type 1), pore-fillings (Type 2) and well-crystallized lath form (Type 3) from the Haengmae Formation, a dolomite–pebble-bearing fine sand-sized dolostone, in South Korea. Based on micro-textural observation, three types of Mg-phengite are associated with crystalline dolomite, and are followed by calcite precipitation as pore-filling, indicating that these should be formed by the influx of a Mg-rich hydrothermal fluid after the deposition of some clastic sediments and before calcite-filling. The structural formula based on $O_{10}(OH)_2$ shows that the number of Mg atoms per formula unit (apfu) of Mg-phengite ranges from 0.00 to 0.70 with no Fe, which is relatively high, compared with the previously reported metamorphic phengites. In REEs mineral chemistry, the Mg-phengites are characterized by the enrichment of REEs and by the particular enrichment of LREEs in the polycrystalline aggregates of Mg-phengite. It strongly suggests that the Mg-phengite should be formed by the infiltration of the highly evolved Mg- and REEs-enriched hydrothermal fluid into the clastic sedimentary rock (Haengmae Formation) as a strata-bound form, syngenetically or during early diagenesis.

Keywords: Mg-phengite; muscovite–celadonite solid solution; Haengmae Formation; infiltration

1. Introduction

Phengite, which is one of the potassic dioctahedral mica, occurs most commonly in metamorphic environments. Compositionally, phengite is an intermediate member of the muscovite $[K_1[Al_2]^{VI}[Al_1,Si_3]^{IV}O_{10}(OH)_2]$—celadonite $[K_1[(Fe^{3+},Al)_1,(Mg,Fe^{2+})_1]^{VI}[Si_4]^{IV}O_{10}(OH)_2]$ solid solution series [1–5]. The mineral chemistry of phengite depends on the composition of the mineralizing fluids [6–9]. Most studies have been conducted to examine the geochemical properties of phengites with the petrographic study. Many researchers have reported phengite series through geochemical analysis by using quantitative compositional data [9–12] and suggested that phengite is mainly formed as metamorphic minerals and a common product of hydrothermal alteration [3,9,13–21]. Tappert et al. [9] distinguished two chemically distinct phengite based on the degree of hydrothermal alteration and explained the systematic change in the mineral chemistry of phengites as an effect of hydrothermal fluid. El Korh et al. [10] linked the content of trace elements in phengite to determine the role of mobile element in fluids from metamorphic conditions. Petrík et al. [11] defined Li-phengite

as Li-bearing high silica variety of muscovite and suggested that Li-phengite and phengite are formed as products of metamorphism during burial diagenesis.

Several studies have been focused on the relationship between phengites and metamorphic environments affected by hydrothermal fluids forming phengites based on the geochemical properties of phengites with the petrographic study. However, only a limited amount of research combined with micro-texture was conducted. In this study, combined with analyses of micro-textural and geochemical studies, we aim to characterize Mg-phengite, which has not been reported in previous studies. Through micro-textural, mineralogical and geochemical analysis, we examine micro-textural types of Mg-phengite and demonstrate how Mg-phengite has a genetic relationship with surrounding mineral assemblages. Based on this work, we expand upon the occurrence of Mg-phengite formed by the infiltration of hydrothermal fluid in the carbonate sedimentary rock and provide evidence to elucidate the process of the sedimentary environment in this study area.

2. General Geology of Mg-Phengite Occurrence Area

The Mg-phengite-series minerals occur in a dolomite–pebble-bearing fine sand-sized dolostone, so-called the Haengmae Formation (Figure 1, [22]). The Haengmae Formation belongs to the Pyeongchang Group, which is the "undifferentiated" Cambrian–Ordovician carbonate sequences in Pyeongchang and Jeongseon area [22,23]. The Haengmae Formation is underlain by the Jeongseon Formation and overlain by the Silurian Heodongri Formation [23–25]. The Haengmae Formation was first, identified in the Jeongseon area [24,26] and was reported later in the western part of the Pyeongchang area [27–29]. It was originally described as a yellowish-brown pebble-bearing limestone, thin layers of limestone and silicic clastic rocks that are severely weathered and poorly lithified [23]. However, a recent study has revealed that the Haengmae Formation is a dolomite–pebble-bearing fine sand-sized dolostone with calcite-fillings [30]. Previous studies for conodont microfossils suggested that the Haengmae Formation indicates the Ordovician age [24,31]. Jang [23] obtained the U–Pb detrital zircon age of ca. 450 Ma from the Haengmae Formation, which suggests that the maximum age of the Haengmae Formation is the Late Ordovician Period.

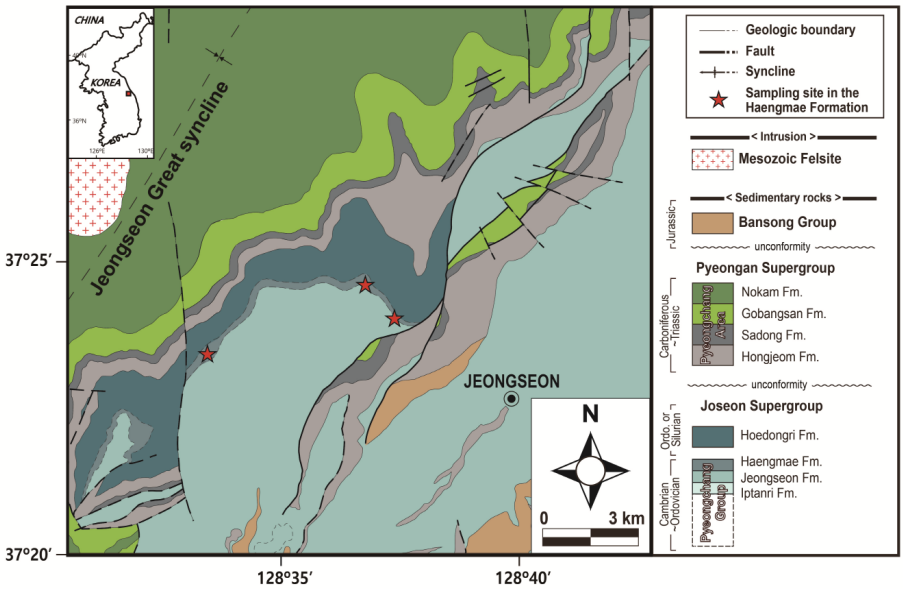

Figure 1. Regional geological map showing the northwestern Taebaeksan Zone of South Korea (modified after [22]). Stars indicate the sampling site in Haengmae Formation.

3. Analytical Methods

Samples were collected from several outcrops showing a typical lithology of the Haengmae Formation. Polished slabs and thin sections were prepared for micro-textural characterization using

polarized light (PL) microscopy, SEM-BSE (scanning electron microscopy with backscattered electron) observation, EPMA-WDS (Electron probe micro analyzer with wavelength dispersive spectroscopy) and LA (Laser Ablation)-ICPMS analyses and powders for X-ray diffraction analysis.

Polarized light microscopic observation was performed for thin sections after alizarin red S staining, which is useful to distinguish calcite from dolomite. SEM-BSE observation experiments were performed for the polished samples after carbon-coated on the surface using a high-vacuum (HV) SEM (JSM-5610LV; JEOL, Ltd.; Tokyo, Japan) and an EDS system (Oxford Instruments, Abingdon, UK) at Yonsei University, Seoul, South Korea. BSE-compo and elemental mapping images were acquired using an EDS system (Oxford Instruments, Abingdon, UK) with a 20 kV of accelerating voltage. X-ray diffraction (XRD) analysis was examined for the bulk and some selected pebbles using a Rigaku Miniflex II XRD system (CuKα radiation) in the step-scan mode (0.02° step, 1 s/step scanning time and 2°–60° 2θ ranges).

Quantitative analysis of major and minor elements was performed using an EPMA-WDS system (JXA-8100; JEOL, Ltd.; Tokyo, Japan) with a 20 keV accelerating voltage, 20 μA beam current and 5-μm-diameter probes with a 4-channel spectrometer at Yonsei University, Seoul, South Korea. The natural mineral standards were used for quantification, and the raw data were corrected using the standard Zinc Application Framework (ZAF) correction. The EPMA was used on nine target elements (Si, Ti, Al, Fe, Mn, Mg, Ca, Na and K). EPMA was also used to observe the micro-textures of the polished samples as well.

Trace elements for the selected area in microscale of phengite were analyzed by a 213-nm-wavelength New Wave UP213 UV laser ablation system and a Thermo Scientific Company X7 ICPMS at the KBSI (Korea Basic Science Institute), Ochang, South Korea. Data were obtained with 30 s dwell time, and the operating conditions were a 10-Hz repetition rate, 25-μm spot-size and 1.313-mJ beam energy. All measurements were conducted using NIST612 glass [32] as external standards and SiO_2 content, determined from EPMA as internal standard. The AMS software from Virginia Tech was selected to calculate the trace element composition.

4. Results

4.1. Characteristics of Haengmae Formation Containing Mg-Phengite

The typical Haengmae Formation containing Mg-phengite is composed of yellowish-brown carbonate rocks with poor lithification and is characterized by containing various types of pebbles (Figure 2A). These pebbles are observed to be scattered in the matrix of the carbonate rock as angular to sub-rounded shapes with several mm to in size and are composed of a large aggregate with microsized dolomite, calcite-dominant rock, phyllitic rock and a white-colored aggregate of phengite with several to tens mm in size (Figure 2D–G).

Based on petrographic microscope observation and X-ray diffraction analysis, the matrix of the carbonate rock was mainly composed of dolomite, quartz, calcite and phengite-series mica. Dolomite is observed in the form of euhedral-shaped growth grains, ranging in size from tens to hundreds of micrometers (Figure 2B,C,G). Quartz shows a well-rounded and well-sorted form with a size of tens of micrometers, which is a typical detrital character (Figure 2B,C). Calcite is a major mineral, but it exists only as fillings between dolomite and quartz grains (Figure 2B,C). Phengite occurs as not only a white-colored aggregate, but also a pore-filling in the matrix (Figure 2G), which will be mentioned in the following part of this study.

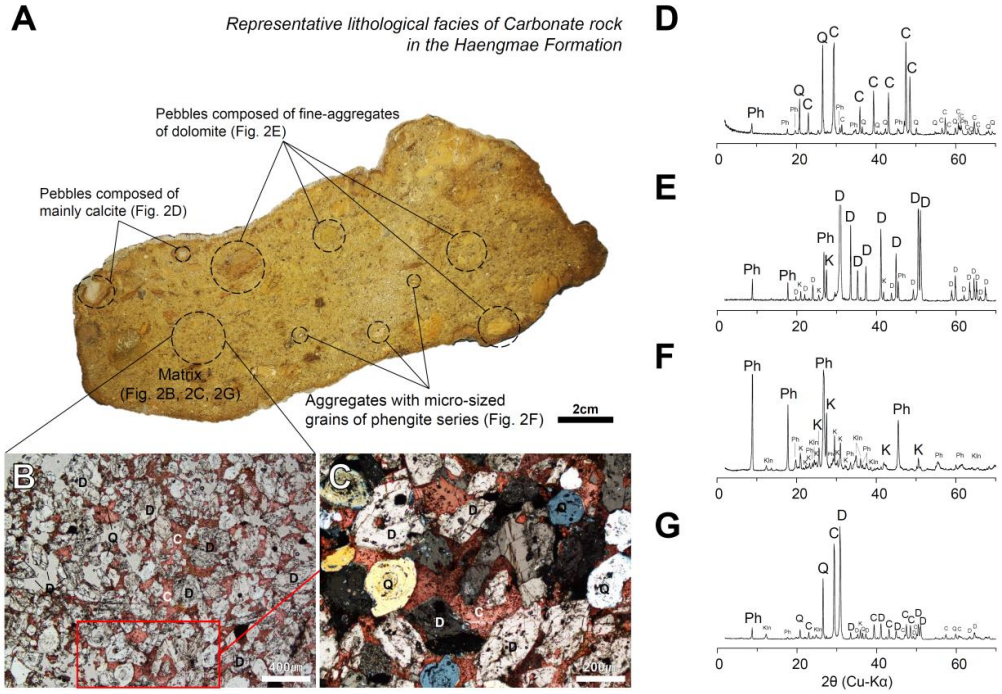

Figure 2. (**A**) Representative lithological facies of carbonate rock in the Haengmae Formation. Polished slab of the typical Haengmae Formation is characterized by the yellowish-brown in color and the various types of pebble, containing a large aggregate with microsized dolomite, calcite-dominant rock, phyllitic rock and a white-colored aggregate of phengite; (**B**) polarized microscopic images of the matrix under plane polarized light (PPL) mode after alizarin red S staining, showing a typical texture composed of single crystalline dolomite, well-rounded and well-sorted quartz grains with calcite fillings, and (**C**) its enlarged image under crossed polarized light (XPL) modes. X-ray diffraction results of (**D**) the pebbles of calcite-dominant rock, (**E**) a large aggregate with microsized dolomite, (**F**) a white-colored aggregate of phengite, and (**G**) the typical matrix. Abbreviations: Q—quartz; K—K-feldspar; Kln—kaolinite; C—calcite; D—dolomite; Ph—phengite.

4.2. Micro-textural Analysis of Mg-Phengite

The most distinct characteristic of phengite is its occurrence as a white-colored aggregate with several to tens mm in size (Figures 2A and 3A). On the results of BSE image, the phengite aggregate is mainly composed of polycrystalline phengite with several hundred micrometers in size (Figure 3A). The polycrystalline phengite exists as fibrous cryptocrystalline with a preferred alignment (Type 1). Element-mapping results of the selected area indicate that the Type 1 phengites can be divided into relatively high-Mg/low-Al Mg-phengite and low-Mg/high-Al one by the relative Mg and Al contents. Micro-textural evidence shows that the low-Mg/high-Al Mg-phengite should be formed later (Figure 3C–F). Fe content was not detected in both phengites (element-mapping result of Fe was not shown in Figure 3). A small amount of K-feldspar and quartz are scattered as anhedral grains in the phengite aggregates (Figure 3C,D,F).

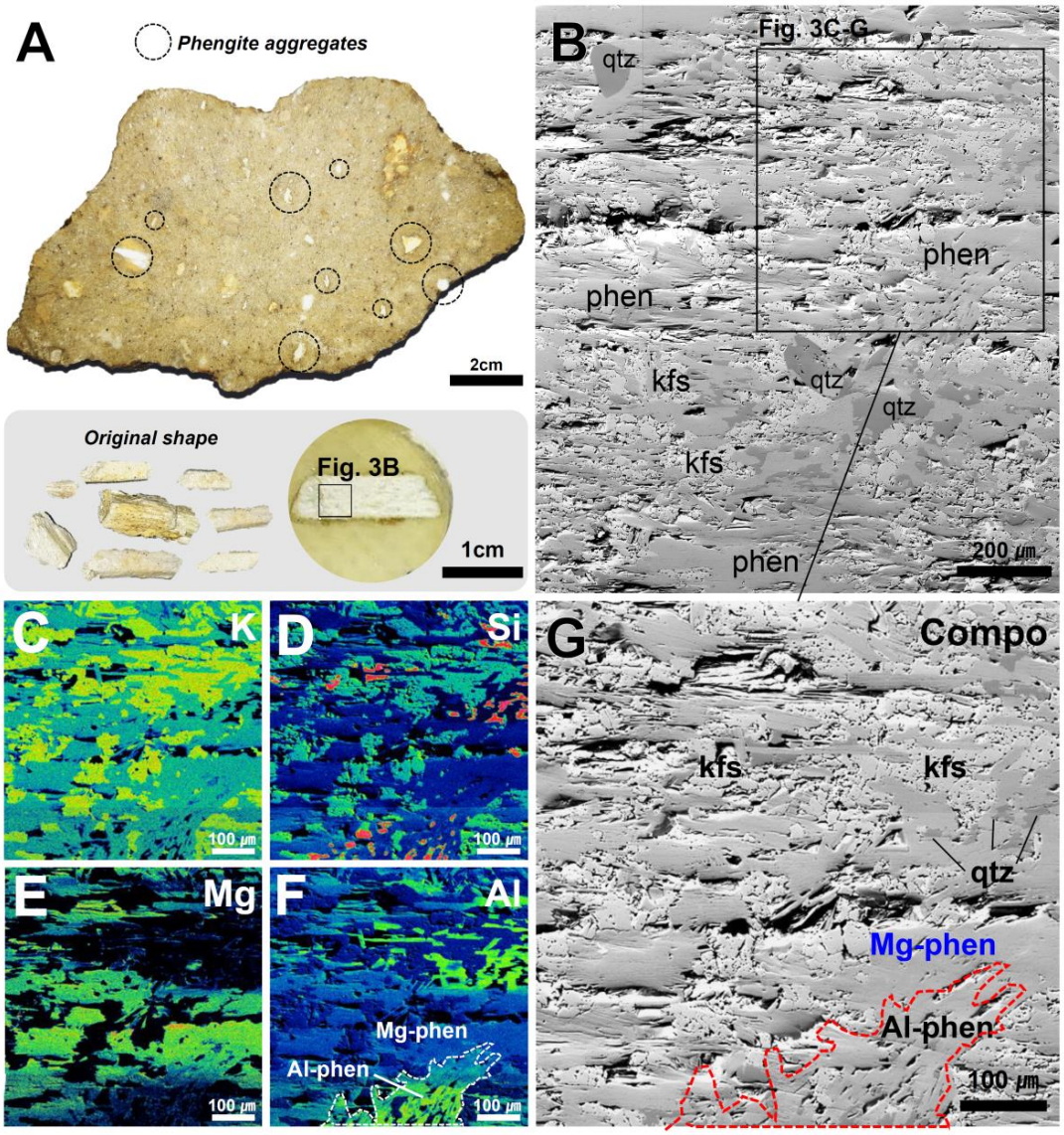

Figure 3. (**A**) Typical phengite aggregates scattered on the polished slab of the typical Haengmae Formation and the separate ones; (**B**) BSE image of the representative phengite aggregate, which is mainly composed of polycrystalline phengite (Type 1) with several hundred micrometers in size with a small amount of quartz and K-feldspar. Element-mapping results of the selected area for (**C**) K, (**D**) Si, (**E**) Mg, and (**F**) Al; (**G**) exaggerated BSE image of the selected part from (**B**). Abbreviations: qtz—quartz; kfs—K-feldspar; Mg-phen and Al-phen—relatively high-Mg/low-Al and low-Mg/high-Al Mg-phengite, respectively.

On the other hand, phengite also occurs as pore-filling aggregates in the matrix (Figure 2G) (Type 2). It shows a typical micro-texture that phengite was precipitated as a filling mineral in the pores between the grains, such as crystalline dolomite, dolomite pebbles, quartz and polycrystalline phengite aggregates, which is followed by calcite filling (Figure 4A–F). Element-mapping results show that the Type 2 phengite is also typical Mg-phengite with no Fe content (Figure 4G–K) (element-mapping result of Fe was not shown in Figure 4). In some samples, the pore-filling phengites (Type 2) are elongated by shearing along with the adjacent dolomite pebble (Figure 5). It is also followed by the calcite-fillings (Figure 5A,B). Element-mapping results show the fine aggregates of the elongated Type 2 Mg-phengite fibers with no Fe content, which is distinctly cross-cut by thin veins of calcite (Figure 5C–H).

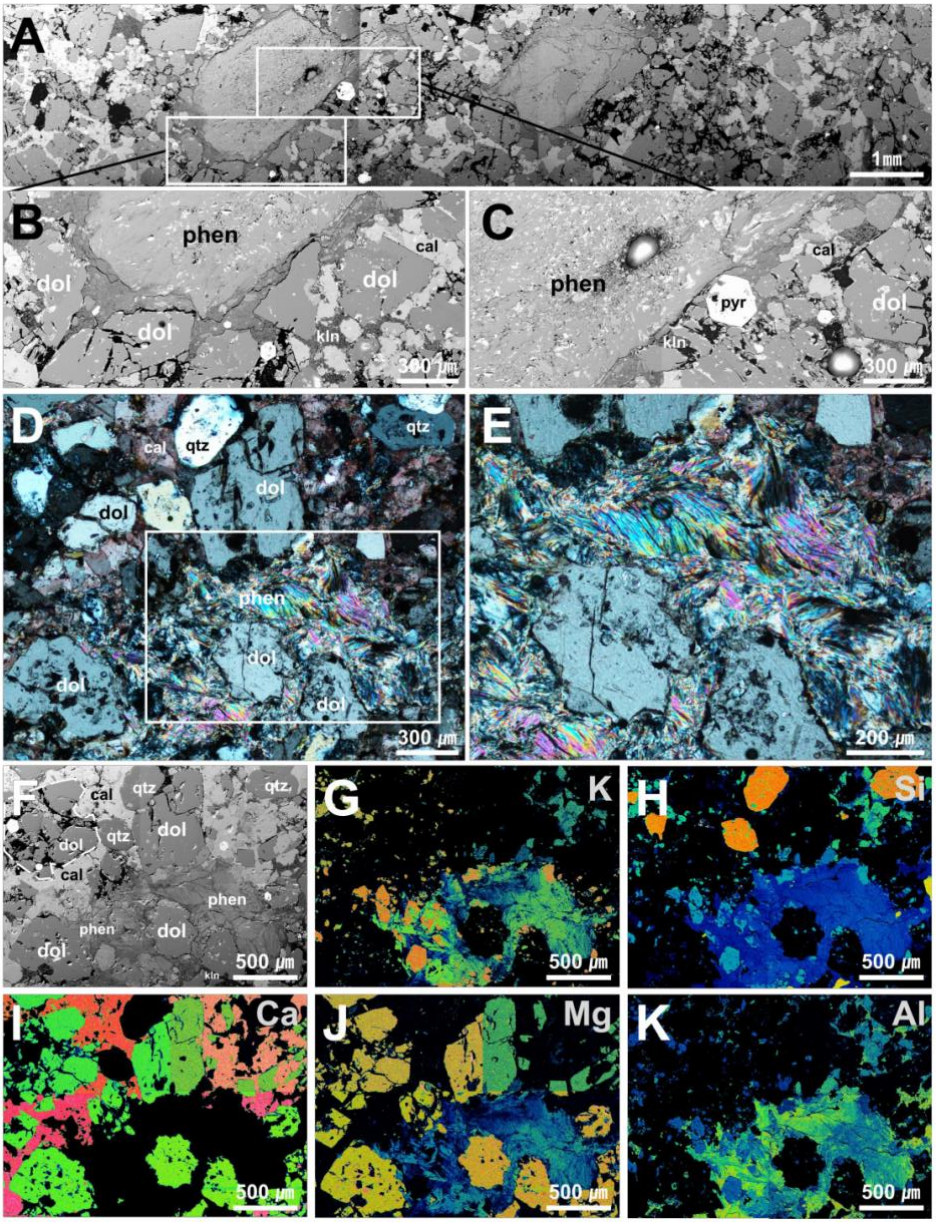

Figure 4. (**A**–**C**) SEM-BSE image of pore-filling phengites (Type 2) among the crystalline dolomite grains and polycrystalline phengite (Type 1) in carbonate rock, which is followed by calcite filling; (**D**,**E**) XPL images of typical pore-filling phengites (Type 2); (**F**) SEM-BSE image of Type 2 phengite for element-mapping and the element-mapping results of the BSE imaging part for (**G**) K, (**H**) Si, (**I**) Ca, (**J**) Mg, and (**K**) Al. Abbreviations: qtz—quartz; cal—calcite; dol—dolomite; phen—phengite; pyr—pyrite; kln—kaolinite.

In some samples, the well-crystallized euhedral to subhedral flaky phengite (Type 3) with 100 to 300 μm in size is also observed between dolomite and quartz grains and around the dolomite pebbles with a grain size greater than 1 mm (Figure 6). It appears as a clustered form in the pore spaces, and these grains have clearly distinguishable boundaries, which cut off the growth of adjacent minerals (Figure 6A–C). Micro-textural evidence shows that the well-crystallized phengite should be formed after pore-filling phengites. Element-mapping results show the typical euhedral to subhedral form of Mg-phengite crystals with no Fe content (not shown in Figure 6), and calcite also fills the pores after the phengite precipitation (Figure 6E–I).

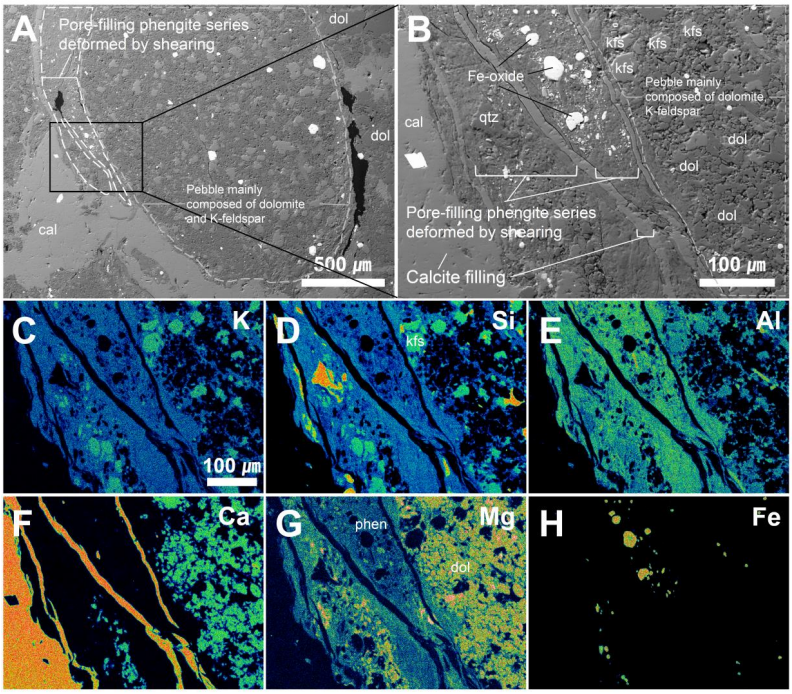

Figure 5. (**A**) SEM-BSE image of pore-filling phengites (Type 2) elongated by shearing along with the adjacent dolomite pebble and followed by the calcite-fillings and its (**B**) exaggerated image. Element-mapping results of the BSE imaging part for (**C**) K, (**D**) Si, (**E**) Al, (**F**) Ca, (**G**) Mg and (**H**) Fe. Abbreviations: qtz—quartz; cal—calcite; dol—dolomite; phen—phengite; kfs—K-feldspar.

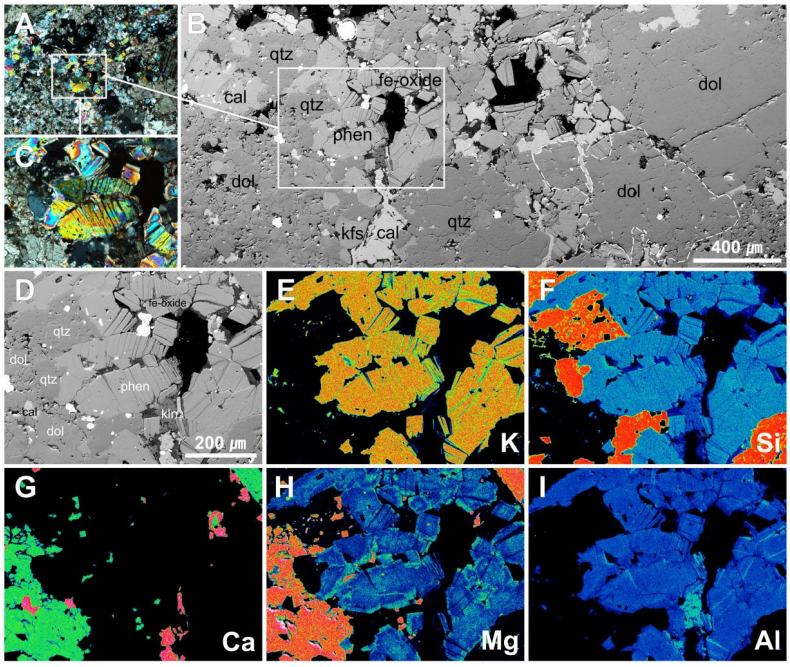

Figure 6. (**A**,**C**) XPL images of typical well-crystallized euhedral to subhedral flaky phengite (Type 3) with 100 to 300 μm in size; (**B**) SEM-BSE image of well-crystallized phengites (Type 3) precipitated around the dolomite pebble, crystalline dolomite and quartz and followed calcite filling; (**D**) SEM-BSE image of Type 3 phengite for element-mapping and the element-mapping results of the BSE imaging part for (**E**) K, (**F**) Si, (**G**) Ca, (**H**) Mg and (**I**) Al. Abbreviations: qtz—quartz; cal—calcite; dol—dolomite; phen—phengite; kfs—K-feldspar.

4.3. Mineral Chemistry of Phengite

The EPMA results of the typical phengite types are summarized in Table 1 and all data are listed in Table S1. The major elements show the typical phengite-series compositions ranging as follows: 44.50–55.86 wt % for SiO_2, 21.05–36.87 wt % for Al_2O_3, 10.60–11.67 wt % for K_2O, 0.00–7.01 wt % for MgO and almost 0.00 wt % for FeO (Table 1 and Table S1). The structural formulae are calculated using 11 oxygens (Table 1).

Table 1. Representative electron probe micro analyzer (EPMA) data of the phengites from the Haengmae Formation and structural formulae calculated using 11 oxygens.

	Polycrystalline Aggregate Type						Pore-Filling Type			Well-Crystallized Type		
	Type 1a * (n = 30)			Type 1b * (n = 50)			Type 2 (n = 50)			Type 3 (n = 30)		
	Min.	Max.	Average	Min.	Max.	Average	Min.	Max.	Average	Min.	Max.	Average
SiO_2	44.50	47.99	45.75	51.06	55.86	52.91	52.10	55.56	53.70	48.66	51.35	49.91
TiO_2	0.00	0.03	0.01	0.00	0.42	0.03	0.00	0.27	0.03	0.13	0.50	0.34
Al_2O_3	30.46	36.87	34.70	21.05	25.95	23.85	21.00	24.53	22.82	26.01	29.12	27.83
FeO	0.00	0.37	0.12	0.20	0.35	0.28	0.19	0.38	0.23	0.08	0.24	0.12
MnO	0.00	0.04	0.01	0.00	0.03	0.00	0.00	0.03	0.01	0.00	0.02	0.00
MgO	0.00	1.98	0.56	4.19	6.46	5.37	4.58	7.01	5.90	3.18	5.05	3.86
CaO	0.00	0.09	0.01	0.00	0.20	0.03	0.00	0.11	0.05	0.07	0.63	0.13
Na_2O	0.02	0.11	0.07	0.00	0.10	0.05	0.02	0.17	0.06	0.11	0.34	0.17
K_2O	10.86	11.58	11.22	11.13	11.67	11.33	10.60	11.63	11.28	10.83	11.32	11.08
sum	87.98	94.55	92.44	93.01	95.25	93.86	92.59	95.45	94.07	92.45	94.82	93.44
Si (IV)	3.05	3.25	3.13	3.47	3.71	3.56	3.54	3.68	3.60	3.31	3.44	3.37
Al (IV)	0.75	0.95	0.87	0.29	0.53	0.44	0.32	0.46	0.40	0.56	0.69	0.63
Sum (IV)	4.00	4.00	4.00	4.00	4.00	4.00	4.00	4.00	4.00	4.00	4.00	4.00
Al (VI)	1.78	1.98	1.92	1.35	1.55	1.45	1.32	1.50	1.40	1.50	1.63	1.59
Ti (VI)	0.00	0.00	0.00	0.00	0.02	0.00	0.00	0.01	0.00	0.01	0.03	0.02
Fe (VI)	0.00	0.02	0.01	0.01	0.02	0.02	0.01	0.02	0.01	0.00	0.01	0.01
Mn (VI)	0.00	0.00	0.00	0.00	0.00	0.00	0.00	0.00	0.00	0.00	0.00	0.00
Mg (VI)	0.00	0.21	0.06	0.42	0.65	0.54	0.46	0.70	0.59	0.32	0.50	0.39
Sum (VI)	1.98	2.00	1.98	1.98	2.02	2.00	1.98	2.03	2.01	1.98	2.04	2.00
Ca	0.00	0.01	0.00	0.00	0.01	0.00	0.00	0.01	0.00	0.01	0.05	0.01
Na	0.00	0.02	0.01	0.00	0.01	0.01	0.00	0.02	0.01	0.01	0.04	0.02
K	0.96	1.00	0.98	0.96	0.99	0.97	0.90	1.00	0.96	0.93	0.98	0.96
Sum	0.98	1.01	0.99	0.98	1.01	0.98	0.91	1.01	0.98	0.97	1.02	0.99

* Type 1a and Type 1b indicate relatively low-Mg/high-Al Mg-phengite and relatively high-Mg/low-Al Mg-phengite, respectively.

Phengite series is a dioctahedral solid solution between two end-members of muscovite $[K_1[Al_2]^{VI}[Al_1,Si_3]^{IV}O_{10}(OH)_2]$ and celadonite $[K_1[(Fe^{3+},Al)_1,(Mg,Fe^{2+})_1]^{VI}[Si_4]^{IV}O_{10}(OH)_2]$. The relation between Al total atoms per formula unit (apfu) versus sum of Si, Mg and Fe (apfu) can define the hetero-valent substitution of $Al^{VI}Al^{IV} \leftrightarrow (Mg,Fe)^{VI}Si^{IV}$ for charge-balancing in the phengite-series solid solution. All data are plotted on the muscovite to aluminoceladonite substitution line with a distinctly different range for each phengite type (Figure 7). The plots of polycrystalline aggregate phengite (Type 1) are clearly divided into two types (Type 1a and 1b), which are due to the distinct difference in Mg and Al contents (Figure 7, Table 1). The plots of pore-filling type phengite (Type 2) are similar to those of Type 1b phengites, whereas those of well-crystallized phengite (Type 3) are plotted in the relatively high-Al region. The number of Mg atoms per formula unit (apfu) of these Mg-phengites ranges from 0.00 to 0.70 with no Fe (Table 1 and Figure 7). Plots on the diagram of Al(VI) versus Si(IV) (Figure 8A) and Mg(VI) versus Si(IV) (Figure 8B) based on atoms per formula unit (apfu) for the Type 1, 2, and 3 phengites strongly indicate the trends of theoretical hetero-valence substitution of $Al^{VI}Al^{IV} \leftrightarrow (Mg, Fe)^{VI}Si^{IV}$ for charge-balancing in the phengite-series solid solution (Figure 8).

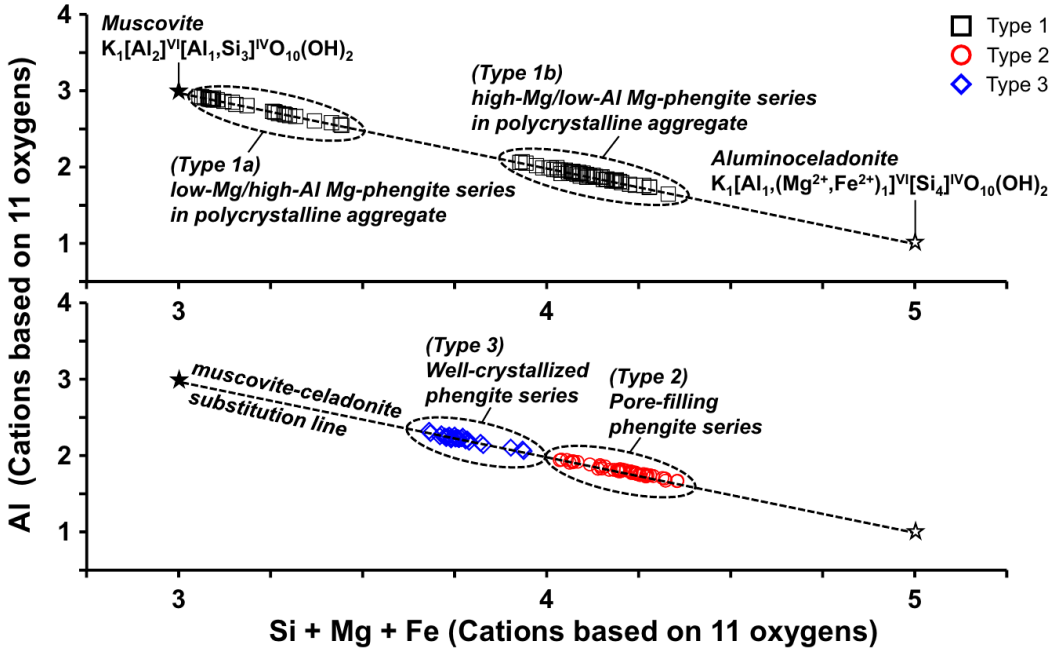

Figure 7. Plots on the diagram of Al total atoms per formula unit (apfu) versus sum of Si, Mg and Fe (apfu) for the Type 1, 2 and 3 phengites from the Haengmae Formation. The dashed line indicates the theoretical hetero-valence substitution of $Al^{VI}Al^{IV} \leftrightarrow (Mg,Fe)^{VI}Si^{IV}$ for charge-balancing in the phengite-series solid solution.

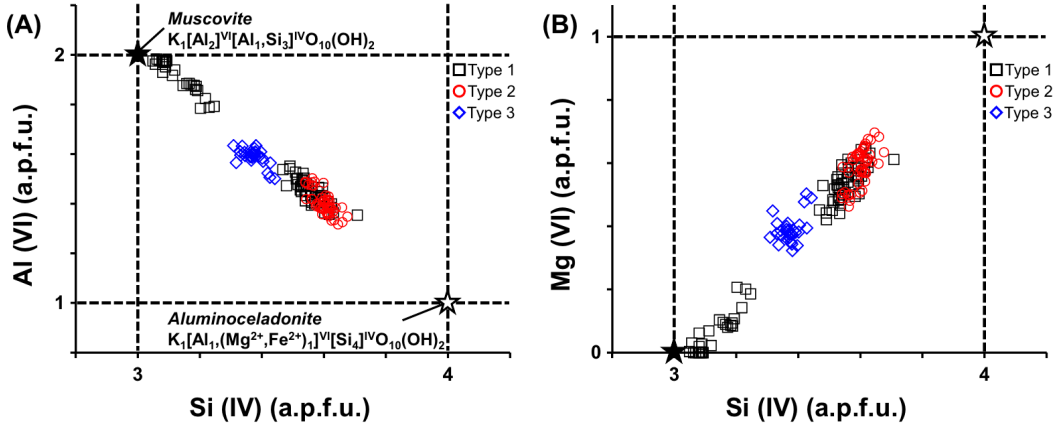

Figure 8. Plots on the diagram of Al(VI) versus Si(IV) (**A**) and Mg(VI) versus Si(IV) (**B**) for the Type 1, 2 and 3 phengites from the Haengmae Formation. The trends show the theoretical hetero-valence substitution of $Al^{VI}Al^{IV} \leftrightarrow (Mg,Fe)^{VI}Si^{IV}$ for charge-balancing in the phengite-series solid solution.

The results of LA–ICP–MS analyses for rare earth elements (REEs) of the phengites from the Haengmae Formation are listed in Table S2, and the chondrite-normalized REE patterns are presented in Figure 9. The characteristics of REEs in the phengites from the Haengmae Formation are summarized as follows: (1) the REE concentrations of the phengites are much higher than those of metamorphic phengites [10], (2) all types of the phengites show a similar pattern in MREE to HREE region, and (3) the polycrystalline phengite (Type 1) as aggregates reveal a distinct LREE-enriched pattern, whereas the pore-filling phengite (Type 2) and well-crystallized phengite (Type 3) reveals a relatively LREE-depleted pattern (Figure 9).

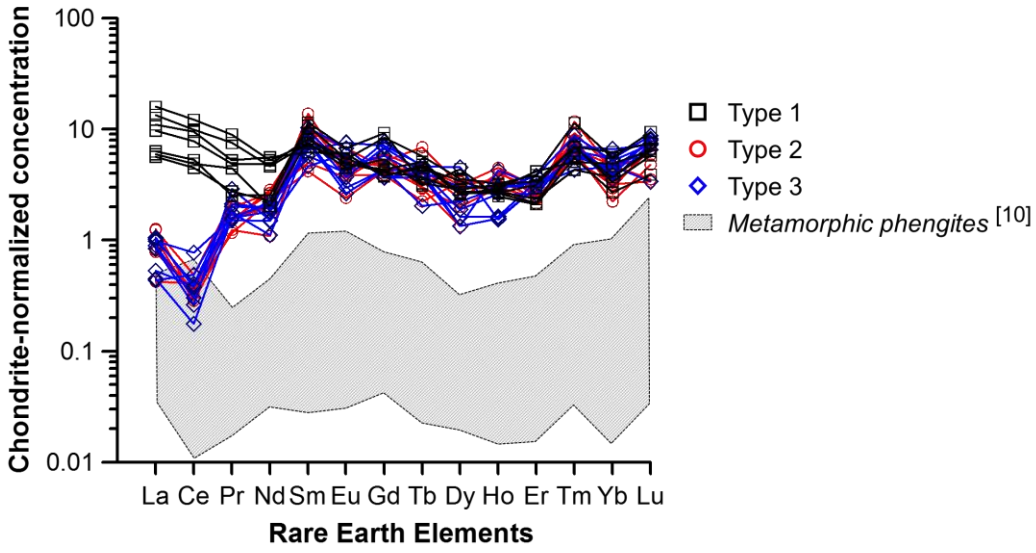

Figure 9. The chondrite-normalized rare earth elements (REEs) patterns of the phengites from the Haengmae Formation. The shadow area indicates the range of REE patterns for the metamorphic phengites [10].

5. Discussion

The three types of phengite series that occurred from the Haengmae Formation are defined micro-texturally as polycrystalline aggregates (Type 1), pore-fillings (Type 2) and well-crystallized lath form (Type 3) (Figures 3–6). These types of phengite series show a typical hetero-valence substitution between $Al^{VI}Al^{IV}$ and $(Mg,Fe)^{VI}Si^{IV}$ for charge-balancing (Figure 8) and contain high Mg (apfu of Mg ranges from 0.00 to 0.70) (Table 1), which is relatively high, compared with the previously reported metamorphic phengites [9–12,33–40]. In particular, there is no Fe in the structure, which is an extraordinary case in common phengite series in the metamorphic environment. Micro-textural evidence and chemical variations in Type 1 phengites (Figure 3C–F) strongly indicate that the Mg-rich fluid would have changed in composition during infiltration through the clastic sediments after input occurred or several different pulses of the hydrothermal fluid input with a difference in Mg-concentration. The Mg-concentration of the fluid should have been low in the later stage and the polycrystalline aggregates of Type 1b and 1a phengites would be formed sequentially through the fluid influx for a relatively long-term. On the other hand, Type 2 and Type 3 phengites would have been formed in an initial stage just after the influx of the fluid. Considering the micro-textural features and Mg-content, Type 2 phengite should be formed earlier than Type 3 one.

The major element chemistry of the phengites in this study is compared with some phengites reported in metamorphic and pegmatitic environments and shown in Figure 10. Muscovite formed in granitic pegmatite zonation or muscovite formed by hydrothermal alteration during the early stages of metamorphism, and unaltered hydrothermal muscovite in granite has a very low degree of $Al^{VI}Al^{IV}$–$Mg^{VI}Si^{IV}$ and $Al^{VI}Al^{IV}$–$Fe^{VI}Si^{IV}$ substitutions, and the octahedral sites are almost filled with Al [36–38] (Figure 10).

Muscovite in a pegmatitic environment, which is a product of extreme granitic fractionation, is included in the muscovite region and is shown in a region with relatively high Fe substitution (Figure 10). Li-phengite, which is mainly formed from granites, greisens and hydrothermal veins, has a higher degree of substitution than muscovite [11]. In the case of other phengites, Mg and Fe partially replace Al site of the octahedral sheet (Figure 10). Partial retrogression of phengite towards muscovite during latter metamorphic events or phengite formation during metamorphic hydrothermal alteration has been reported [9,10,12,39,40]. On the other hand, the Mg-phengite in this study with no Fe is an unusual case. In addition, the phengites are commonly associated with crystalline dolomite,

and are followed by calcite precipitation as pore-filling (Figures 4–6). Considering that the Haengmae Formation is a clastic rock containing various pebbles and detrital quartz, the phengites should have been formed by the influx of a Mg-rich hydrothermal fluid after the deposition of some clastic sediments and before calcite-filling.

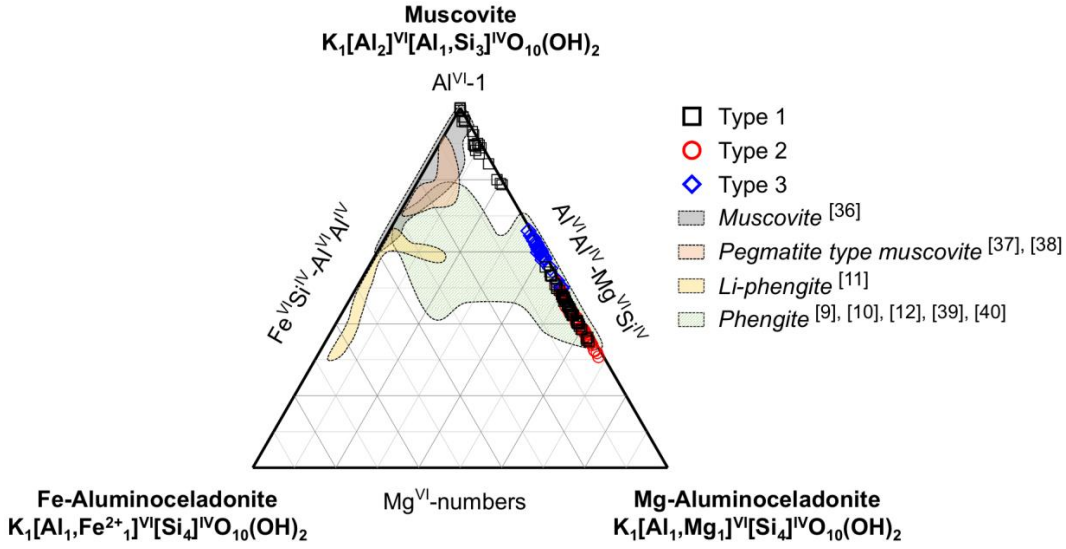

Figure 10. Ternary diagram among muscovite–Fe-aluminoceladonite–Mg-aluminoceladonite. Type 1, 2 and 3 phengites are plotted and compared with some reference muscovites and phengites. Reference muscovite, pegmatite type muscovite, Li-phengite and phengite are plotted.

In REEs mineral chemistry, the Mg-phengites are characterized by the enrichment of REEs rather than some metamorphic phengites [10]. In particular, LREEs are much more enriched in Type 1 phengite than the other types (Figure 9). LREEs are relatively incompatible elements with micas and then they are normally more enriched in the later stage of fluid/melt. Therefore, the enrichment of LREEs in Type 1 phengite strongly indicates that this type of phengite should have precipitated in the relatively late stage (for Type 1a, low-Mg/high-Al Mg-phengite), and/or be continuously re-equilibrated with the fluid after being precipitated (for Type 1b, high-Mg/low-Al Mg-phengite). In addition, the REEs results suggest that the Mg-phengite should be formed by the infiltration of the highly evolved Mg- and REEs-enriched hydrothermal fluid and particularly LREE-enriched hydrothermal fluid in the later stage into the clastic sedimentary rock (Haengmae Formation) as a strata-bound form, syngenetically or during early diagenesis.

Based on the above, a genetic sequence model of Mg-phengite in the Haengmae Formation is presented in Figure 11. In the initial stage, detrital clasts, including detrital quartz grains, dolomite pebbles and rock fragments, etc.; were deposited on the basin being formed by syn-sedimentary growth faults (Figure 11A). Crystalline dolomite and Mg-phengite were precipitated by the influx and infiltration of the highly evolved Mg- and REEs-enriched hydrothermal fluid into the clastic sediments or sedimentary rock (Haengmae Formation) as a strata-bound form, syngenetically or during early diagenesis (Figure 11B). The sedimentary environment changed to shallow marine and calcite precipitated, which filled the pore space of the Haengmae Formation as cement (Figure 11C) as shown in Figures 4–6 and the continuous deposition of calcite formed the Hoedongri Formation in the later stage (Figure 11D).

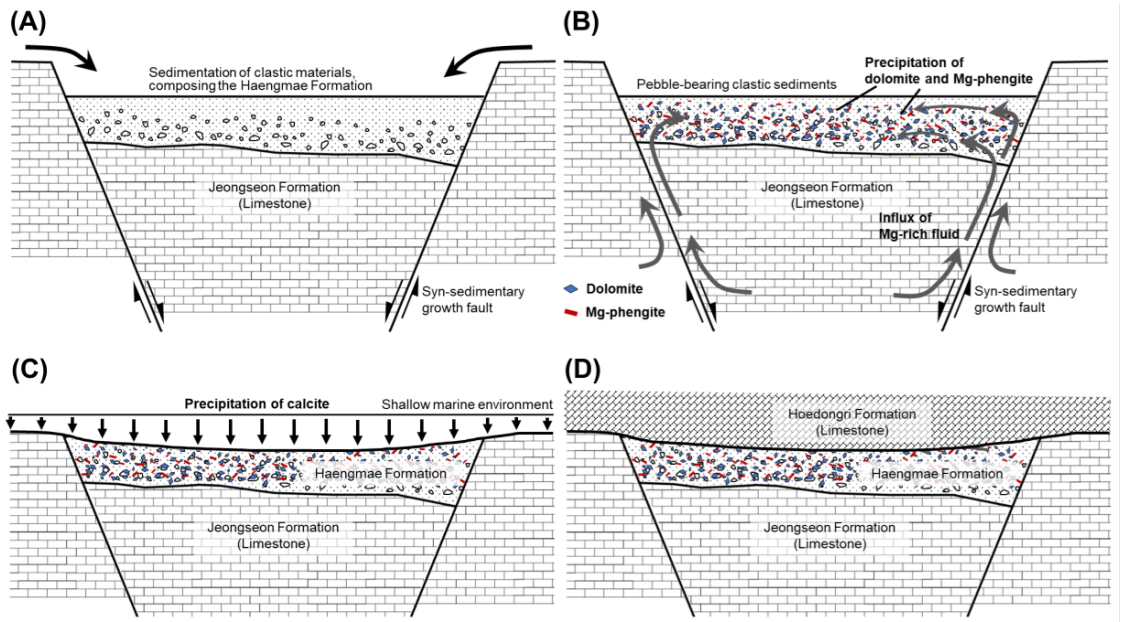

Figure 11. A genetic model for Mg-phengite in the Haengmae Formation. (**A**) In the initial stage, detrital clasts, including quartz, dolomite pebbles and rock fragments, etc.; were deposited on the basin being formed by syn-sedimentary growth faults; (**B**) Dolomite and Mg-phengite were precipitated by the influx and infiltration of the highly evolved Mg- and REEs-enriched hydrothermal fluid into the clastic sedimentary rock (Haengmae Formation) as a strata-bound form, syngenetically or during early diagenesis; (**C**) The sedimentary environment changed to shallow marine and calcite was precipitated, which filled the pore spaces of the Haengmae Formation as cement, and (**D**) the continuous deposition of calcite formed the Hoedongri Formation in the later stage.

6. Summary

A hydrothermal-originated authigenic Mg-phengite-series mineral occurred as polycrystalline aggregates (Type 1), pore-fillings (Type 2) and well-crystallized lath form (Type 3) from the Haengmae Formation, a dolomite–pebble-bearing fine sand-sized dolostone, South Korea. The Mg-phengites are associated with crystalline dolomite and are followed by calcite precipitation as pore-filling. The number of Mg atom per formula unit (apfu) ranges from 0.00 to 0.70 with no Fe. The Mg-phengites are characterized by the enrichment of REEs and by the particular enrichment of LREEs in the polycrystalline aggregates of Mg-phengite.

It strongly suggests that the Mg-phengite should be formed syngenetically by the infiltration of the highly evolved Mg- and REEs-enriched hydrothermal fluid into the clastic sedimentary rock (Haengmae Formation) as a strata-bound form.

Supplementary Materials: The following are available online at http://www.mdpi.com/2075-163X/10/8/668/s1, Table S1: EPMA analysis of phengite, Table S2: LA-ICPMS analysis of phengite.

Author Contributions: Conceptualization, C.P.; N.K. and Y.S.; data curation, C.P. and N.K.; formal analysis, C.P.; funding acquisition, Y.S.; investigation, C.P.; N.K. and S.-J.C.; methodology, C.P. and Y.S.; project administration, Y.S.; supervision, Y.S.; visualization, C.P.; writing—original draft, C.P.; writing—review & editing, Y.S. All authors have read and agreed to the published version of the manuscript.

Funding: This study was funded by Korea Meteorological Administration Research and Development Program under Grant KMI2018–01910.

Acknowledgments: We would like to appreciate the reviewers and editor who reviewed this study and also thank to those gave help to us in the editing process. In addition, we are sending great thanks to the Korea Basic Science Institute for supporting experiment.

Conflicts of Interest: The authors declare no conflicts of interest.

References

1. Schaller, W.T. An interpretation of the composition of high-silica sericites. *Mineral. Mag.* **1950**, *29*, 406–415. [CrossRef]
2. Foster, M.D. Correlation of dioctahedral potassium micas on the basis of their charge relations. *U. S. Geol. Surv. Bull.* **1956**, *1036-D*, 57–67.
3. Ernst, W.G. Significance of phengitic micas from low-grade schists. *Am. Mineral.* **1963**, *48*, 1357–1373.
4. Rieder, M.; Cavazzini, G.; D'yakonov, Y.S.; Frank-Kamenetskii, V.A.; Gottardi, G.; Guggenheim, S.; Koval, P.W.; Mueller, G.; Neiva, A.M.; Radoslovich, E.W.; et al. Nomenclature of the Micas. *Clays Clay Miner.* **1998**, *46*, 586–595. [CrossRef]
5. Rieder, M.; Cavazzini, G.; D'yakonov, Y.D.; Frank-Kamenetskii, V.A.; Gottardi, G.; Guggenheim, S.; Müller, G.; Neiva, A.M.R.; Radoslovich, E.W.; Robert, J.L.; et al. Nomenclature of the micas. *Can. Mineral.* **1998**, *36*, 905–912. [CrossRef]
6. Meunier, A.; Velde, B. Phengitization, sericitization and potassium–beidellite in a hydrothermal-altered granite. *Clay Miner.* **1982**, *17*, 285–299. [CrossRef]
7. Eberl, D.D.; Srodon, J.; Lee, M.; Nadeau, P.H.; Northrop, H.R. Sericite from the Silverton caldera, Colorado: Correlation among structure, composition, origin, and particle thickness. *Am. Mineral.* **1987**, *72*, 914–934.
8. Hitzman, M.W.; Orekes, N.; Einaudi, M.T. Geological characteristics and tectonic settings of Proterozoic iron oxide (Cu–U–Au-REE) deposits. *Precambrian Res.* **1992**, *58*, 241–287. [CrossRef]
9. Tappert, M.C.; Rivard, B.; Giles, D.; Tappert, R.; Mauger, A. The mineral chemistry,near-infrared, and mid-infrared reflectance spectroscopy of phengite from theOlympicDam IOCG deposit, South Australia. *Ore Geol. Rev.* **2013**, *53*, 26–38. [CrossRef]
10. El Korh, A.; Schmidt, S.T.; Ulianov, A.; Potel, S. Trace element partitioning in HP-LT metamorphic assemblages during subduction-related metamorphism, Ile de Groix,France: A detailed LA-ICP-MS study. *J. Petrol.* **2009**, *50*, 1107–1148. [CrossRef]
11. Petrík, I.; Čík, Š.; Miglierini, M.; Vaculovič, T.; Dianiška, I.; Ozdín, D. Alpine oxidation of lithium micas in Permian S-type granites (Gemeric unit, Western Carpathians, Slovakia). *Mineral. Mag.* **2014**, *78*, 507–533. [CrossRef]
12. Gambino, F.; Borghi, A.; d'Atri, A.; Martire, L.; Cavallo, M.; Appolonia, L.; Croveri, P. Minero-petrographic characterization of Chianocco Marble employed for Palazzo Madama Façade in Turin (Northwest Italy). *Sustainability* **2019**, *11*, 4229. [CrossRef]
13. Crowley, M.S.; Roy, R. Crystalline solubility in the muscovite and phlogopite groups. *Am. Mineral.* **1964**, *49*, 348–362.
14. Cibin, G.; Cinque, G.; Marcelli, A.; Mottana, A.; Sassi, R. The octahedral sheet of metamoprhic 2M1-phengites: A combined EMPA and AXANES study. *Am. Mineral.* **2008**, *93*, 414–425. [CrossRef]
15. Frey, M.; Hunziker, J.C.; Jager, E.; Stern, W.B. Regional distribution of white K-mica polymorphs and their phengite content in the central Alps. *Contrib. Mineral. Petrol.* **1983**, *83*, 185–197. [CrossRef]
16. Gouzu, C.; Itaya, T.; Takeshita, H. Interlayer cation vacancies of phengites in calcshists from the Piemonte zone, wester Alps, Italy. *J. Mineral. Petrol. Sci.* **2005**, *100*, 142–149. [CrossRef]
17. Massonne, H.J.; Schreyer, W. Phengite geobarometry based on the limiting assemblage with K-feldspar, phlogopite, and quartz. *Contrib. Mineral. Petrol.* **1987**, *96*, 212–224. [CrossRef]
18. Shau, Y.-H.; Feather, M.E.; Essene, E.J.; Peacor, D.R. Genesis and solvus relations of submicroscopically intergrown paragonite and phengite in a blueschist from nothern California. *Contrib. Mineral. Petrol.* **1991**, *106*, 367–378. [CrossRef]
19. Velde, B. Phengite micas: Synthesis, stability, and natural occurence. *Am. J. Sci.* **1965**, *263*, 886–913. [CrossRef]
20. Velde, B. Si^{+4} content of natural phengites. *Contrib. Mineral. Petrol.* **1967**, *14*, 250–258. [CrossRef]
21. Roberts, D.E.; Hudson, G.R.T. The Olympic Dam copper–uranium–gold deposit, Roxby Downs, South Australia. *Econ. Geol.* **1983**, *78*, 799–822. [CrossRef]
22. Jang, Y.; Cheong, H.J. Structural geometry of the Pyeongchang-Jeongseon Area of the Northwestern Taebaeksan Zone, Okcheon Belt. *Econ. Environ. Geol.* **2019**, *52*, 541–554, (In Korean with English abstract).
23. Jang, Y. Structural Style of the Phanerozoic Polyphase Orogenic Belt in the Western Taebaeksan Zone, Okcheon Belt, Korea: Insights from Multidisciplinary Analyses. Ph.D. Thesis, Yonseic University, Seoul, Korea, 2018.

24. Cheong, C.H.; Lee, H.Y.; Koh, I.S.; Lee, J.D. A study on stratigraphy and sedimentological environments of the lower Paleozoic sequences in South Korea (Chiefly in Jeongseon Area). *J. Natl. Acad. Sci. Repub. Korea (Nat. Sci.)* **1979**, *18*, 123–159. (In Korean)
25. Lee, H.Y. Discovery of Silurian conodont fauna from South Korea. *J. Geol. Soc. Korea* **1980**, *16*, 114–123.
26. Son, C.M.; Cheong, J.G. Geology of the Northwestern part of Pyeongchang district, Gangweon-do, Korea. *J. Geol. Soc. Korea* **1971**, *7*, 103–116. (In Korean with English abstract).
27. Kim, J.M. A Study on Stratigraphy and Paleontology of the Lower Paleozoic Sequence in the Kogilri-Daehwari Area, Pyeongchang-Gun, Kangweon-Do (Chiefly by Means of Conodont Study). Master's Thesis, Yonsei University, Seoul, Korea, 1982. (In Korean with English abstract).
28. Seo, K.S. A Study on Stratigraphy and Paleontology of the Lower Paleozoic Sequences in the Daewhari and Anmiri Area, Pyeongchang-Gun, Kangwon-Do (Chiefly by Means of Conodont Study). Master's Thesis, Yonsei University, Seoul, Korea, 1983. (In Korean with English abstract).
29. Yi, M.S. A Study on Stratigraphy and Paleontology of the Lower Paleozoic Sequence in the Bangrimri and Jujinri Area, Pyeongchang-Gun, Kangweon-Do (Chiefly by Means of Conodont Study). Master's Thesis, Yonsei University, Seoul, Korea, 1983. (In Korean with English abstract).
30. Park, C.; Kim, N.; Song, Y. Micro-textural and mineralogical Characteristics of the Haengmae Formation. In Proceedings of the 2019 Joint International Conference of the Geological Science and Technology of Korea, Jeju, South Korea, 17–19 April 2019; p. 236. (In Korean).
31. Choi, S.-J. A Study on Biostratigraphy and Micropaleontology of the Hoedongri and Haengmae Formation in Pyeonganri Area, Pyeongchang-Gun, Gangwon-Do. Master's Thesis, Yonsei University, Seoul, Korea, 1980. (In Korean with English abstract).
32. Pearce, N.; Perkins, W.; Westgate, J.; Gorton, M.; Jackson, S.; Neal, C.; Chenery, S. A compilation of new and published major and trace element data for NIST SRM 610 and NIST SRM 612 glass reference materials. *Geostand. Newsl.* **1997**, *21*, 115–144. [CrossRef]
33. Bishop, B.P.; Bird, D.K. Variation in sericite compositions from fracture zones within the Coso Hot Springs geothermal system. *Geochim. Cosmochim. Acta* **1987**, 1245–1256. [CrossRef]
34. Evans, A.M. Ore geology and industrial minerals: An introduction (third edition). *Blackwell Sci.* **1993**, *1993*, 1–389.
35. Yang, K.; Huntington, J.F.; Cudahy, T.J.; Mason, P.; Scott, K.M. Spectrally mapping the compositional variation of white micas in hydrothermal systems and the application in mineral exploration. In Proceedings of the 2001 Geoscience and Remote Sensing Symposium, International Geoscience and Remote Sensing Symposium, Sydney, Australia, 9–13 July 2001; pp. 3294–3296.
36. Psyrillos, A.; Howe, J.H.; Manning, D.A.C.; Burley, S.D. Geological controls on kaolin particle shape and consequences for mineral processing. *Clay Miner.* **1999**, *34*, 193–208. [CrossRef]
37. Deveaud, S.; Millot, R.; Villaros, A. The genesis of LCT-type granitic pegmatites, as illustrated by lithium isotopes in micas. *Chem. Geol.* **2015**, *411*, 97–111. [CrossRef]
38. Hulsbosch, N.; Hertogen, J.; Dewaele, S.; André, L.; Muchez, P. Alkali metal and rare earth element evolution of rock-forming minerals from the Gatumba area pegmatites (Rwanda): Quantitative assessment of crystal-melt fractionation in the regional zonation of pegmatite groups. *Geochim. Cosmochim. Acta* **2014**, *132*, 349–374. [CrossRef]
39. Di Vincenzo, G.; Tonarini, S.; Lombardo, B.; Castelli, D.; Ottolini, L. Comparison of 40 Ar/39 Ar and Rb–Sr data on phengites from the UHP Brossaco-Isasca unit (Dora Maira Massif, Italy): Implications for dating white mica. *J. Petrol.* **2006**, *47*, 1439–1465. [CrossRef]
40. Aoki, K.; Windley, B.F.; Sato, K.; Sawaki, Y.; Kawai, T.; Shibuya, T.; Kumagai, H.; Suzuki, K.; Maruyama, S. Chemical composition and K-Ar age of phengite from Barrovian metapelites, Loch Leven, Scotland. *J. Geol. Soc. Jpn.* **2013**, *6*, 437–442. [CrossRef]